A study of electron scattering through noise spectroscopy

Kumar, M.

4

DETECTION OF VIBRATION MODE SCATTERING IN ELECTRONIC SHOT NOISE

Manohar KUMAR, Remi AVRILLER, Alfredo Levy YEYATI, Jan van RUITENBEEK

Generally, current shot noise is measured at low bias currents, and it reflects the transmission probability of the electrons. Here we present the first measurement at bias currents above the phonon energy of the system, i.c. a chain of Au atoms. The onset of phonon emission processes is signaled by an abrupt jump in differential conductance. One should expect a sign of this change to be visible in shot noise. Indeed, a distinct signature in the current shot noise signal is observed due to inelastic scattering as a linear deviation from the Levitov- Lesovik classical shot noise. In accordance to recent theoretical predictions the sign of the inelastic signal, i.e., the signal due to vibration excitations depends on the transmission probability, becoming negative below a certain transmission value. We argue that the negative contribution to noise arises from coherent two-electron processes mediated by electron-phonon scattering and the Pauli exclusion principle.

Parts of this chapter have been published in Physical Review Letters **108**, 146602 (2012).

4.1 INELASTIC NOISE SPECTROSCOPY

THE inelastic interaction of electrons with vibrons leads to abrupt changes in the conductance. This effect has been studied extensively[1–6]. This technique is widely used in transport spectroscopies, *i.e.* point contact spectroscopy (PCS) and inelastic electron tunneling spectroscopy (IETS). Transport spectroscopy has been used to identify the nature of the species in the point contact[7–12]. Shot noise, as the second cumulant of the current, is another fundamental quantity of quantum transport. Together with conductance spectroscopy noise spectroscopy can help to characterize in detail atomic and molecular junctions. It can provide valuable insights in the fundamental nature of the processes taking place in quantum transport. An elusive property in molecular electronics is the lattice temperature of the molecule in the contact, for which shot noise may provide quantitative information. Shot noise S for a single channel conductor is proportional to $\tau(1-\tau)$, where τ is the transmission probability of the channel. This noise should also show the signature of the inelastic electron-phonon interactions. Recently Refs. [13–15] have predicted the presence of an inelastic shot noise signature of electron-phonon interaction in their studies on a simple model of a molecular junction having single resonant level, symmetrically couple to both leads, and for weakly interacting conduction electrons with a single phonon mode. In case of a small decay rate of the vibration modes into phonon modes of the leads a non-equilibrium vibron occupation is expected[14, 16–19]. The fluctuations in the non-equilibrium vibronically excited state affects the dynamics of the traversing electrons. Hence the measurement of this non-equilibrium vibronic population in noise measurement could reveal the lattice temperature of the quantum device. Au atomic chains, forming a simple test bed for the inelastic scattering in conductance, have been used here as a first test system for inelastic scattering effects in noise spectroscopy. We have looked into, both, equilibrated and non-equilibrated vibronic interactions on the conduction electrons in Au atomic chains.

4.2 AU ATOMIC CONTACT FORMATION

GOLD atomic chains were formed at liquid helium temperatures using mechanically controllable break junctions (MCBJ). This technique permits freshly exposing clean Au metal electrodes, which are then pressed gently together such as to form a cold weld of atomic size. This contact can be repeatedly made and broken such that the contact changes its cross section atom-by-atom. In the last stages of breaking Au contacts the atoms have been found to spontaneously arrange into a linear strand of up to 8 atoms in length. At the start of the experiments the sample chamber is pumped to $\sim 10^{-5}$mbar before cooling down in liquid helium. The chamber is fitted with active charcoal for cryogenic pumping such that the pres-

sure in the chamber drops below measurable values when reaching the base temperature, which is between 5 and 8K. Once cold and under vacuum the Au sample wire is first broken by mechanical bending of the substrate. By relaxing the bending the broken wire ends can be rejoined and the contact can be adjusted with sub-atomic precision by means of a piezo-electric actuator[20].

4.2.1 DC CHARACTERIZATION

A first step in characterizing the quality of the junction is taken by recording conductance histograms. Contacts are repeatedly made and broken, controlled by the piezo voltage that regulates the substrate bending of the mechanically controllable break junction device. While gently breaking the Au atomic contacts the conductance of the junction decreases in steps due to the atom-by-atom reduction in contact size. The points of the digitized traces of conductance are collected into a histogram and the counts are plotted as a function of the conductance. Conductance histograms such as shown in figure(4.1 a) are obtained by combining typically 2000 conductance breaking traces. The first peak at $1G_0$ represents the average conductance of a contact of a single Au atom in cross section, which has a lot of weight because of the long atomic chains being formed. This can be seen from the traces shown in the inset of figure(4.1 a) having long plateaus at $1G_0$. On these plateaus the conductance is changing very little while the contact is being stretched. This is explained by the formation of the long atomic chains and, upon further stretching the contact, the chains finally break to form clean vacuum tunnel junctions, shown by the diminishing counts at lower conductance in the conductance histogram.

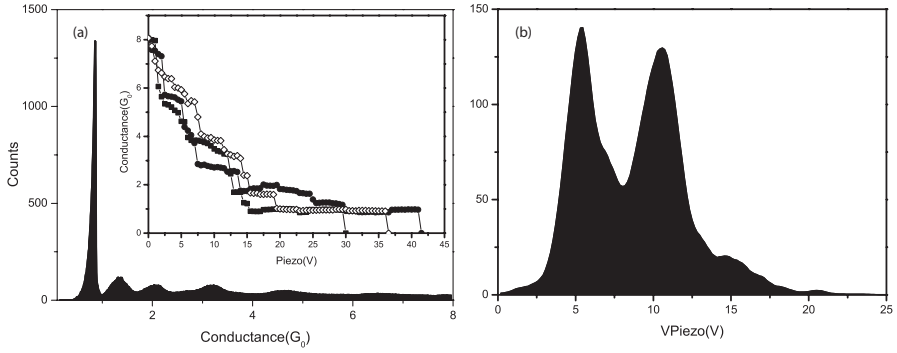

FIGURE 4.1: The dc characterization of Au atomic contacts: (a) A conductance histogram recorded for 2000 conductance traces. Typical conductance traces are shown in the inset. (b) A length histogram recorded for the same conductance traces. The two prominent peaks show the presence of 2 and 3 atom long atomic chains forming predominantly. The inter-peak distance gives the calibration factor of $1.96 V/Å$

In the conductance breaking traces a last conductance plateau near $1G_0$ signals the formation of a junction of only a single atom in cross section. The value of the length of this plateau for several hundreds of breaking cycles is collected into a length histogram, see figure(4.1 b). The histogram is obtained by combining 2000 traces and recording the length of the conductance plateaux with conductances between 0.8 and $1.1G_0$, i.e. in the range of the first conductance peak in figure(4.1). The length axis is given in units of the voltage on the piezo element, where the proportionality constant is 1.96 V/Å. The histogram is consistent with the earlier work of Untiedt *et al.* [21]. This length histogram shows several peaks with a separation consistent with the inter-atomic distance in a chain of Au atoms. The first four peaks can be interpreted as the lengths corresponding to chains of 2, 3, 4 and 5 atoms. Still longer chains have diminished counts and hence are not always visible in the length histogram.

4.2.2 AC CHARACTERIZATION

The ac characterization of Au atomic contacts has been done using lockin measurements. A small amplitude modulation sine signal of 2mV amplitude and 2.3kHz frequency is used for these lockin measurements. The electrical circuit used for the lockin measurement is shown in figure (3.5). Point contact spectroscopy signals for a perfectly transmitting conductor are expected to show a step down feature in the conductance at the vibration mode energy. This is a known concept and has been briefly described in section (3.4.2). In a ballistic conductor, due to electron-phonon interaction, electrons lose energy by emitting a phonon of energy $\hbar\omega_{k_F}$, and in the process are get scattered backwards. This backscattering of the traversing electrons is seen as a decrease in the conductance at the finite voltage $V_{ph} = \hbar\omega_{k_F}$ [22]. For perfectly transmitting atomic contacts one expects a similar phenomenon to be seen in their differential conductance measurements. Having a single *s* valence orbital and a conductance around $1G_0$ Au atomic chains show a nearly perfect transmission. The differential conductance measurement of figure (4.2) for such a contact indeed shows a step-down feature. The scattering on the vibration mode is seen typically as a drop of about 1% in the conductance [23]. The point of extremum in the second derivative of the current gives a measure of the value of this vibronic energy and its amplitudes gives the electron-vibron interaction strength. Although Au atomic chains permit many vibration modes only the longitudinal mode with the largest moment has a significant cross section for inelastic electron scattering [1, 24]. The longitudinal character of the mode of the vibronic signal can be confirmed by looking at figure (4.3). Here, we have measured the differential conductance for various stages of stretching of the contact. The second derivative of the current clearly shows a decrease in the vibronic energy and an increase in the electron-vibron interaction strength. This is in accor-

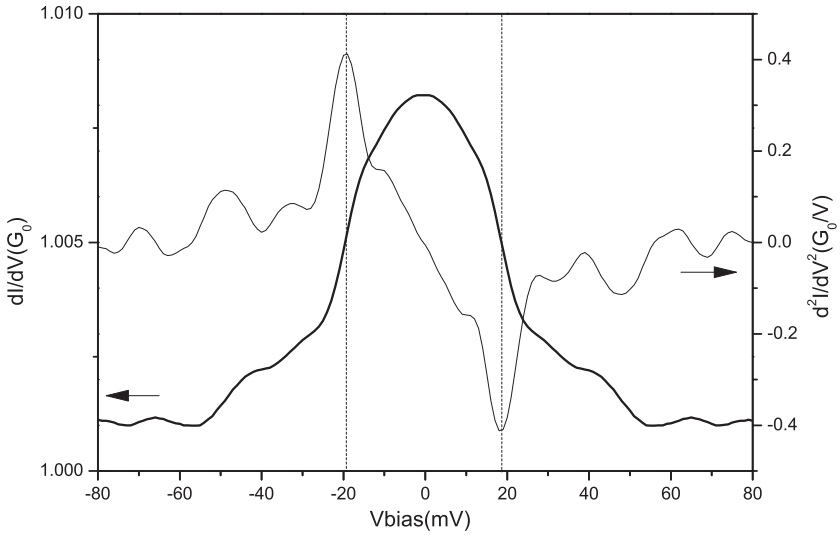

FIGURE 4.2: The ac characterization of Au atomic contacts: The differential conductance of a Au atomic contact (bold curve, left scale) shows a step-down feature at both polarities of the voltage bias. The second derivative of the current (light curve, right scale) shows a dip and a peak at at these positions, at ±19meV at positive and negative bias voltage. The positions of these extrema correspond to the vibron energy in the Au atomic contact.

dance with the longitudinal nature and is due to the softening of the interatomic bond strength upon stretching of the contact. The finite size of the chain, its mechanical coupling to the leads and the finite temperature, lead to broadening of the step feature in the contact. Upon stretching of the contact the corrugation of the potential seen by the electrons increases which leads to a much sharper change in the conductance at the vibronic energy [5].

These features are more pronounced in longer chains as compared to shorter chains. For longer chains the effective change in the vibronic energy with stretching is much larger than for shorter chains. In shorter chains the strong mechanical coupling of the chain with the leads give rise to a strong broadening of the vibration resonance due to fast decay into bulk phonons, which smears out the inelastic signature in the differential conductance. It is also possible to have more than one vibrational mode coupling to the traversing electrons [24]. In our experiment we focus on the longitudinal mode coupled to the electrons in the chain. Hence, for our experimental studies we have pulled Au atomic chains of 3 atoms or longer, and done all point contact spectroscopy and noise spectroscopy on these.

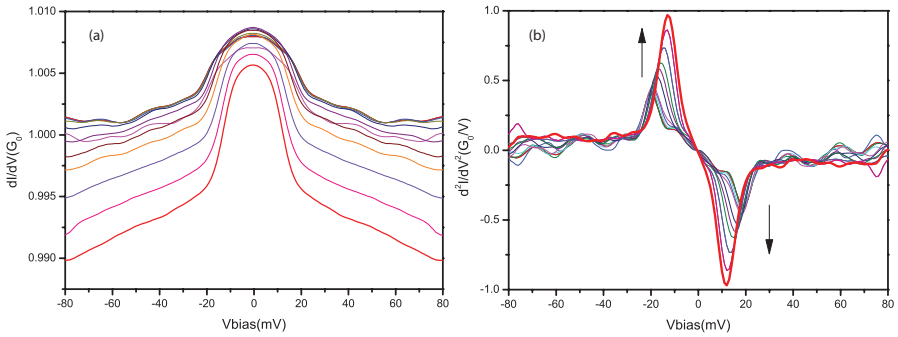

FIGURE 4.3: Stretching dependence of the inelastic electron-vibron interaction energy in Au atomic contacts: (a) Differential conductance measurement on a 4 atom long Au atomic chain at various stages of stretching, in steps of 0.2Å. The green curve shows the starting atomic contact configuration and the red curve shows the final contact, just before breaking. (b) The second derivative of the current shows the evolution of the vibronic energy upon stretching of the contact.The effective rate of change in the vibronic energy is 1.9meV/Å. the color code is the same as that for the differential conductance.

4.3 SHOT NOISE SPECTROSCOPY

THE shot noise studies on the Au atomic contacts are done using a low frequency cross-spectrum analysis technique. The detailed measurement scheme and circuit diagram is shown in figure (3.8). The noise spectra were recorded in a window from 250Hz to 100kHz. An example of such spectra is given in figure (4.4 a). At the low-frequency end of the spectrum one observes an increase in the spectrum above the white noise level due to a $1/f$-like noise contribution, the amplitude of which varies between different junction settings, which has been attributed to defect fluctuations in the leads. This part of the spectrum is ignored for the analysis, but it influences the accuracy of the determination of the white noise power. At the high-frequency end of the spectrum a roll-off is seen, with a characteristic frequency of about 30kHz that is due to the RC time constant of the stray capacitance of the leads in combination with the junction resistance. First, the thermal noise is recorded at zero bias, and after recording noise at several bias settings the zero bias noise is recorded once more (labeled as $0V_r$). The thermal noise level corresponds to a temperature of 6.3K, which agrees within the accuracy of the temperature measurement with a reading of 6.1K, as obtained from a Ruthenium Oxide 10kΩ resistance thermometer. After correction for the roll-off with a single RC time constant the spectra become white above 10kHz, figure (4.4 b). The thermal noise (at zero bias) is subtracted, which explains the negative values in the data fluctuations for the lowest currents. The data points are projected in the form of a histogram, shown at the right, and the level of white noise is obtained from the

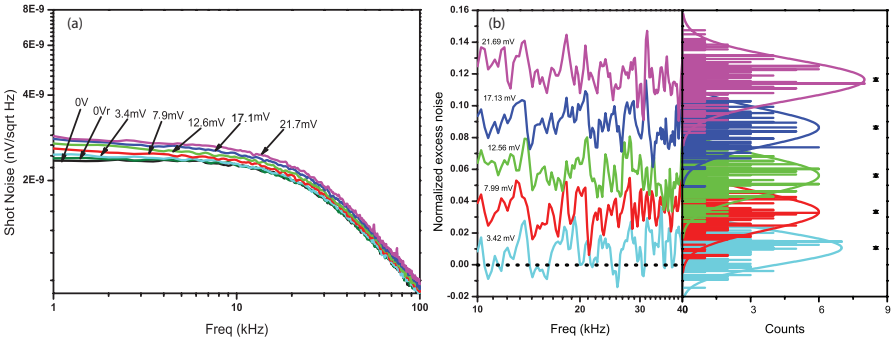

FIGURE 4.4: The raw noise data for a Au atomic contact and its analysis: (a) Noise spectra for a Au atomic chain of ~ 3 atoms in length having a conductance $G = 0.987 G_0$ at a temperature of $T = 7.95$ K. The roll off in the spectra is seen at 32.5kHz (b) Noise after subtracting the thermal noise and correcting for the RC roll off.

center of the histogram for each voltage bias. The points and error bars at the right indicate the position and accuracy of the noise as determined from a Gaussian fit to the histograms. The mean noise value is plotted in reduced axis format to obtain the Fano factor, as shown in figure (4.5) (for an explanation of this procedure see section 3.5.3). The Fano factor calculated from the reduced axis plot for this contact is $F = 0.135 \pm 0.004$.

We recorded noise for over 450 atomic configurations formed using 5 different Au wire MCBJ devices. For each configuration we recorded 25 bias voltage settings in steps of about 1mV. We discarded those data for which the scatter in the reduced-axis plot is larger than 3% and those for which the measured thermal noise at the end of the measurement series differs by more than 2% of the starting value. The scatter is mostly due to contributions of $1/f$ -noise interfering with the white spectrum. Changes in thermal noise may result from changes in the resistance of the contact. Figure (4.6) shows the results for the Fano factor for many such atomic chains as measured for bias voltages below 10mV, and plotted against the conductance as done for instance by Kumar *et al.* [25]. Most atomic chain junctions have a conductance slightly below $1G_0$, but somewhat smaller values frequently occur because of scattering on defects in the leads [26]. All data in figure (4.6) fall close to the black solid line, which is the expected dependence for a single conductance channel, as given by equations (1.28) and (1.27). This clearly shows that Au atomic chains agree with a model of single-channel Landauer conductors.

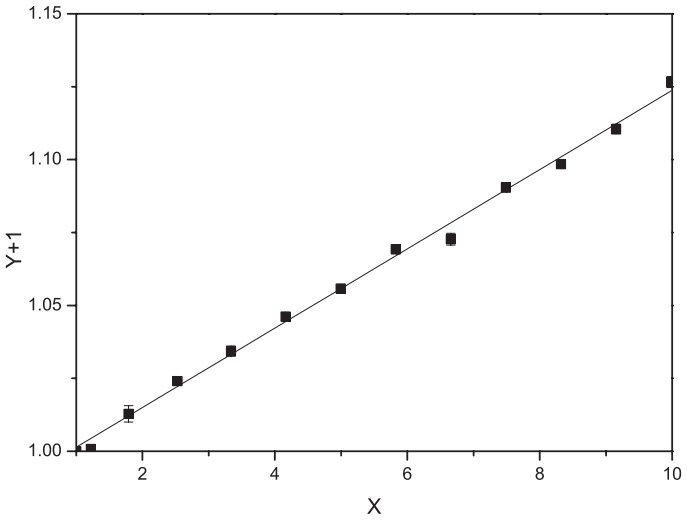

FIGURE 4.5: Determination of the Fano factor from shot noise measured on an Au atomic contact: The mean noise value as obtained from figure (4.4 b) represented in a reduced axis plot. From the slope of this reduced axis plot we obtain a Fano factor of $F = 0.135 \pm 0.004$.

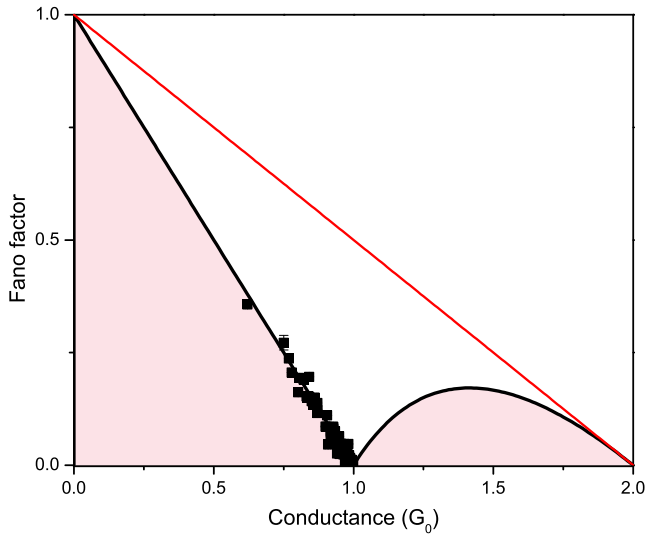

FIGURE 4.6: Fano factor plot for Au atomic contacts: Noise measurements on over 450 atomic configurations formed using 5 different Au wire MCBJ devices. Here we are showing the Fano factor obtained on all these contacts[1]. The Fano factors for all atomic contacts lie on the line $F = 1 - \tau$, *i.e.* on the theoretical limit of minimum Fano factor that is attained only for a single spin-degenerate Landauer conductor.

4.4 INELASTIC VIBRONIC SCATTERING IN NOISE

THE inelastic scattering on vibron modes is seen as a drop of about 1% in the conductance measurements. For Au chains these vibration modes can attain values between about 10mV and 20mV, which varies due to the softening of the bonds with the applied strain in the atomic wire [24], as was discussed in section (4.2.2). For such systems inelastic scattering should also affect shot noise. Most noise measurements on atomic and molecular conductors have been focused on the low bias regime. Here we will look into the noise above the vibronic energy of the Au atomic chain. Figure (4.7a) shows the differential conductance and noise measurement for a Au atomic chain of 4 atoms long. The differential conductance shows the step down feature at the vibronic energy as expected. The second derivative shows a peak and dip feature at about 20mV in both negative and positive bias regime, giving the vibronic energy of the atomic chain. Figure (4.7b) shows the noise power *w.r.t.* the bias voltage upto 28mV. The small curvature at low bias voltage below 3mV is due to the crossover from thermal noise to non-equilibrium noise. Above 3mV the noise power closely follows the expected linear dependence. The red curve is a fit to equation(1.28) and gives a Fano factor $F_1 = 0.020 \pm 0.002$, which agrees with the zero bias conductance $G = 0.98G_0$ for a single conductance channel, within the accuracy of 1% in G [27]. Above 20mV we observe a sudden kink in the noise signal, which matches the energy of the vibration mode seen in figure (4.7a). If we take the slope above the kink

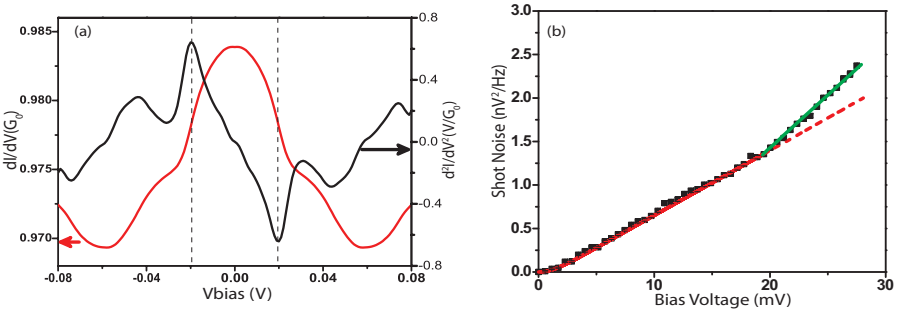

FIGURE 4.7: Inelastic scattering in conductance and noise in a Au atomic contact: The differential conductance (left axis) measurement and its derivative (right axis) on a 4 atom long Au atomic chain. The second derivative was computed numerically. The peak at 20.0 ± 0.4mV signals the onset of scattering by a vibration-mode. (b) Shot noise as a function of bias for the same atomic contact as in (a). The red curve is a fit to the equation(1.28) upto 20mV. The Fano factor $F_1 = 0.020 \pm 0.002$ agrees with the conductance of $G = 0.98G_0$ in (a). The broken red curve is an extrapolation of the fit. The green line is linear fit for the data above 20mV.

to define a modified Fano factor F_2 the relative change in Fano factor is given as $\delta F/F = (F_2 - F_1)/F_1 = \pm 0.90$. We interpret this kink as evidence of an inelastic scattering contribution to shot noise. This interpretation was further tested, and the results are shown in figure (4.8).

Figure (4.8) shows data for seven different chain configurations, plotted as $Y(V)$ vs. $X(V)$. For G close to 1 G_0 (lowest curves) we find a positive correction above the kink. Note the curve with $G = 1.00G_0$, which shows zero noise ($F = 0$) until a kink appears when reaching the vibration mode energy. Remarkably, for $G < 0.95G_0$ the correction above the kink has the opposite sign. The observed dependence is linear in $X(V)$, above and below the kinks, within the experimental accuracy. In some cases we observe a second kink at still higher bias voltages (not shown here), but for the moment we limit attention to the first kink only.

Figure (4.9) shows the position of the steps in the differential conductance against the observed position of the kink in the reduced-axis plot. The kink position in the shot noise is obtained by extrapolating the linear deviation in shot noise due to inelastic scattering and the fit to the equation(1.28). The intersection of these two extrapolated lines gives the position of kink in the shot noise. The derivative of the symmetrized differential conductance curve gives the vibron energy of the Au atomic contact. The difference between the position of the vibron energy in the differential conductance and its symmetric part is incorporated in the error analysis of the vibron energy.[2] The uncertainty and the scatter in the mode energy are due to the difficulty of removing the contributions by conductance fluctuations from the differential conductance. Despite the large uncertainties, a clear trend is observed and the data lie close to the line 1:1. This observation provides strong support for the interpretation of the kink in the noise data as being due to inelastic scattering on vibration modes of the system.

The relative change in the Fano factor for a set of about 120 measurements is shown in figure (4.10), plotted as a function of the transmission probability τ. For τ close to 1 exclusively positive values for $\delta F/F$ are found, while for $\tau < 0.95$ only negative values occur, confirming the trend observed in figure (4.8).

While the effect of inelastic scattering on vibration modes in atomic-size systems has been extensively analyzed theoretically [4, 23, 28, 29] the generalization of these studies to noise properties has only recently started [13–15]. Most of these studies are based on a minimal model corresponding to a single resonant molecular level E_d coupled to the left and right leads by tunneling rates, Γ_L and Γ_R, interacting with a localized vibration mode with frequency ω_0 and a coupling parameter λ. This model, schematically depicted in the inset of figure (4.10), is adequate

[2] Asymmetric coupling in the atomic chain with the leads could also give rise to asymmetry in the differential conductance.

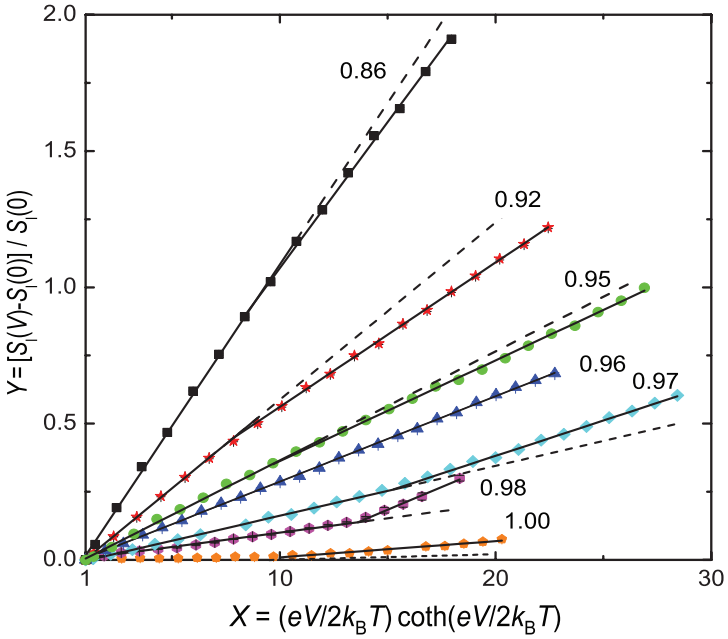

FIGURE 4.8: Kink in shot noise for a range of transmission values of Au atomic chain: In this reduced axis plot the data below the vibron energy are described by a linear dependence (fitted with a solid line up to the kink, and extrapolated by a dashed line). The slope of this line gives the Fano factor. The transmission probability obtained from the conductance is shown as a label to each curve. Above the phonon energy a new linear dependence is observed. The kink is towards higher slope when the transmission probability τ is close to 1. For τ below 0.94 we observe a reduced slope.

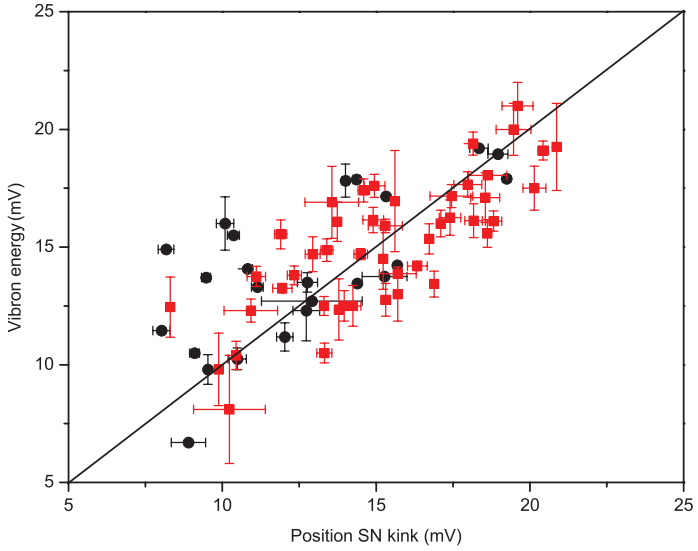

FIGURE 4.9: Correlation between the position of the kink in shot noise and the vibron energy measured using second derivatives of the current: The phonon energy as observed in the differential conductance plotted as a function of the position of kink in the shot noise. The line shows the expected 1:1 relation. Red and black points are for positive and negative kinks, respectively.

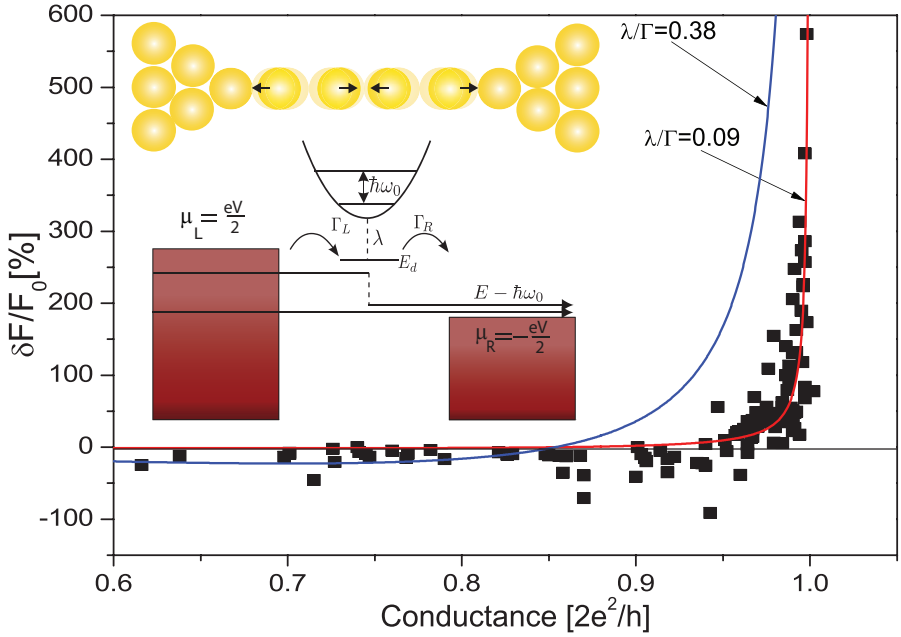

FIGURE 4.10: Distribution of the observed change in the Fano factor at the kink, plotted as a function of the conductance. The points are obtained for different realizations of Au atomic chains. For conductance (*i.e.* transmission $\sim \tau$) close to 1 we find exclusively positive values for $\delta F/F$. Below a cross over regime near $G = 0.95G_0$ only negative values are observed. The curves are obtained from the theory of [13–15], for fixed values of the inelastic scattering strength λ. Inset: The top part illustrates the atomic chain configuration and the vibration mode involved in the scattering. The lower part sketches an example of a two-electron process giving rise to reduction of the Fano factor: two electrons injected from the left lead at different energies tend to compete for the same outgoing state after the emission of a phonon (see section (A.2.2) for further explanation)

for representing a nanosize junction in the regime $\Gamma_{L,R} \gg \omega_0$.

The effect of the phonon mode in the electronic noise properties has been analyzed up to second-order in λ, which is reasonable when the step in the conductance due to inelastic scattering is at most a few percent, see figure (4.7). When the energy dependence of the transmission can be neglected, $\tau(E) \simeq \tau(0)$, the analysis simplifies, and for the zero temperature and positive voltages, the inelastic correction to the noise becomes [13].

$$\delta S_I \simeq \frac{e^2}{h}\left(\frac{\lambda}{\Gamma}\right)^2 \tau^2 \left\{2(1-\tau)(1-2\tau)eV + (8\tau^2-8\tau+1)(eV-\hbar\omega_0)\theta(eV-\hbar\omega_0)\right\} \quad (4.1)$$

where the transmission probability at the Fermi energy is given by $\tau = 4\Gamma_L\Gamma_R/(E_d^2 + \Gamma^2)$ with $\Gamma = \Gamma_L + \Gamma_R$. This expression clearly predicts a crossover from a positive to a negative correction in the noise as the transmission is reduced from the unitary limit. A positive correction due to inelastic scattering giving additional shot noise, such as observed for τ close to 1, is quite intuitive. However, a negative correction such as observed for lower transmission values cannot be understood in simple terms. Eq.(4.1) indicates that the crossover from positive to negative correction is predicted at $\tau_\pm = 1/2 \pm 1/2\sqrt{2}$. The higher crossover point, relevant for the present data set, is $\tau_+ \simeq 0.854$. The microscopic processes contributing to inelastic noise in Eq.(4.1) can be classified into one-electron and two-electron processes, i.e. $\delta S^{(in)} = \delta S_{1e}^{(in)} + \delta S_{2e}^{(in)}$ (see section(A.2.2)). While $\delta S_{1e}^{(in)}$ scales as τ^2 and is thus always positive, the two electron contribution $\delta S_{2e}^{(in)}$ scales as $\{-8\tau^3(1-\tau)\}$ and thus it is always negative[13]. This behavior can be qualitatively understood as arising from the Pauli principle as illustrated by the diagram in the inset of figure (4.10). In this diagram two electrons are injected from the left lead with energies E and $E - \hbar\omega_0$ within the interval $(-V/2, +V/2)$. If the higher energy electron emits a phonon it would tend to occupy the same outgoing state as the other electron. This process would thus be blocked at perfect transmission. Additionally, this process tends to reduce the noise by narrowing the energy distribution of the outgoing electrons. The solid curves in figure (4.10) show the calculated dependence of $\delta F/F$ as a function of τ for two fixed choices of electron-vibron scattering strength λ. The variation of the data can be largely attributed to variations in λ for different chain configurations. There appears to be a trend of λ growing when τ decreases below 1. The crossover in the data to negative values for δF appears at higher τ than expected. The fluctuations in the background of the differential conductance indicate that our assumption of an energy independent transmission may need to be relaxed. Such energy dependence modifies the theory for inelastic scattering but may also affect the linearity of the Fano plots directly, i.e. the usual elastic component of the noise. We have used the measured differential conductance curves to estimate the size of this energy dependence, and have calculated the bias dependence of the noise numerically. Figure (4.11) shows fits to representative data sets (see also sections (A.3.1) and (A.3.2)). It demonstrates that the curves can be correctly described with reasonable values for the parameters, and that the corrections due to the energy dependence of τ to the elastic noise are modest in these cases (see Appendix (A.2.2)).

We also looked into the symmetry of the position of kink in noise and the relative change in the Fano factor due to inelastic scattering *w.r.t.* bias voltage polarity. Figure (4.12) shows a noise measurement for both bias polarities on a Au atomic contact and a Au-O-Au molecular junction. The elastic Fano factors F_1 for positive

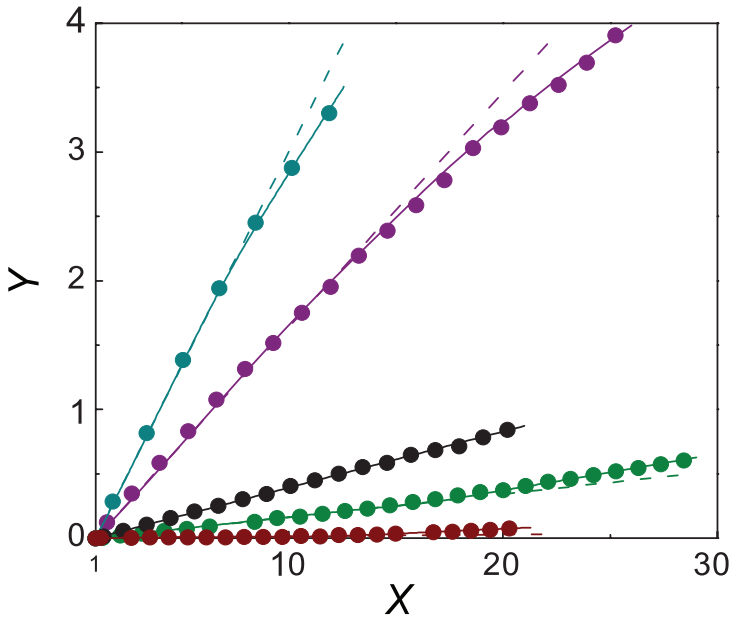

FIGURE 4.11: Theoretical fit of the shot noise data taking energy dependence into consideration: The fits of the theory include the energy dependence of the transmission as estimated from the dI/dV signals (full curve). The broken lines show the linear extrapolation of the zero-bias curve. The values for the zero-bias transmission τ and the inelastic scattering strength are (from top to bottom): $\tau = 0.669$, $\lambda = 0.35\Gamma$; $\tau = 0.818$, $\lambda = 0.20\Gamma$; $\tau = 0.956$, λ undetermined; $\tau = 0.981$, $\lambda = 0.11\Gamma$; $\tau = 0.998$, $\lambda = 0.08\Gamma$.

and negative biases are equal within the experimental error. However, the deviation in noise due to inelastic scattering is different for the positive and negative bias regimes. Also, the kink positions at positive and negative biases for both contacts are different[3]. This may be attributed to an asymmetry in the coupling factor for the atomic chain with the left lead and right lead, $\Gamma_L \neq \Gamma_R$. It is interesting to note that in case of the Au-O-Au chain the inelastic correction in noise is positive for τ as low as 0.91. For Au atomic contacts a negative correction in noise is seen for $\tau < 0.95$. We do not have enough data to identify the cross over regime for Au-O-Au, but our limited data suggests that the cross over may shift somewhat for

[3]The kink in noise for Au-O-Au is seen at $v_+ = 12.7$mV and $v_- = 11.76$mV. This is quite a low energy, which is to be associated with the Au-O-Au atomic chain structure. The derivative of the differential conductance of this particular contact shows extrema at 59meV and 9meV. The high energy mode is related to the presence of a light element in the chain. An example of the differential conductance and its derivative for Au-O-Au is shown in figure (**??**). The inelastic scattering in noise shown in (b) is related to a vibronic mode involving Au atoms, not just oxygen.

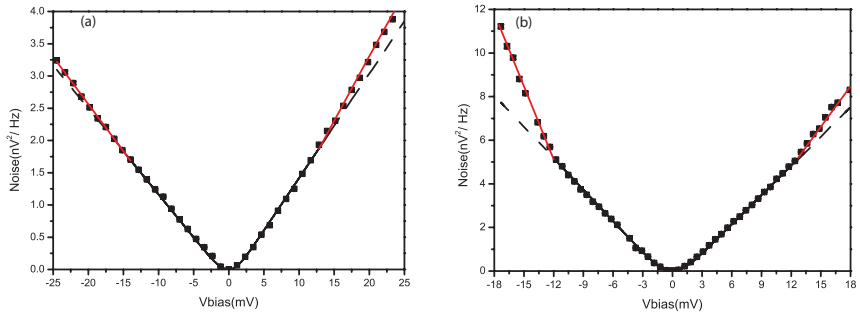

FIGURE 4.12: Inelastic noise for both bias polarities: The noise is measured in both bias polarity regime. (a) Au atomic chain with a conductance of $G = 0.94G_0$. The Fano factor was calculated using the reduced axis plot, giving Fano factors for positive bias of $F_1 = 0.044$ and $F_2 = 0.057$, and for negative bias $F_1 = 0.040$ and $F_2 = 0.043$. (b) Noise measured on a Au-O-Au atomic chain with a conductance of $G = 0.911G_0$. The Fano factors for positive bias are $F_1 = 0.091$ and $F_2 = 0.138$ and for negative bias $F_1 = 0.098$ and $F_2 = 0.25$.

various realizations of atomic chains. The few high bias measurements obtained for the Au-O-Au system are consistent with our observation of a kink in the noise at the vibron energy (see figure (4.9)). The relative change in Fano factor at positive bias and at negative biases are different in the two examples shown and this could be due to asymmetric coupling of the atomic chains to the leads contact [30]. The differential conductance curve for the Au-O-Au chain shows signatures of at least two vibrons due to gold and oxygen in the chain. It would be worthwhile to investigate the coupling of both vibronic signals to the traversing electrons using noise spectroscopy, but this must await the completion of a set-up for higher bias noise measurements.

4.5 NON-EQUILIBRIUM VIBRONIC SIGNATURES IN NOISE

THE inelastic interaction of the electrons with local vibron (vibrons localized within the chain) depends on the electron tunneling rate Γ, the vibronic energy $\hbar\omega_0$, the electron-vibron coupling strength λ, and the vibron relaxation rate η. Depending upon the interplay between these parameters different atomic contacts show different strengths of inelastic signatures in shot noise. As an example, the dependence on λ/Γ is illustrated in figure (4.10). The inelastic signals can be broadly classified in two groups: those for equilibrated vibrons with $\eta \gg \lambda^2\omega_0/\Gamma$ and those for non-equilibrated vibrons with $\eta \ll \lambda^2\omega_0/\Gamma$. The experimental results and the analysis shown above have been assumed to be in the equilibrated vibron limit. The traversing electron dissipates energy into a localized vibron mode

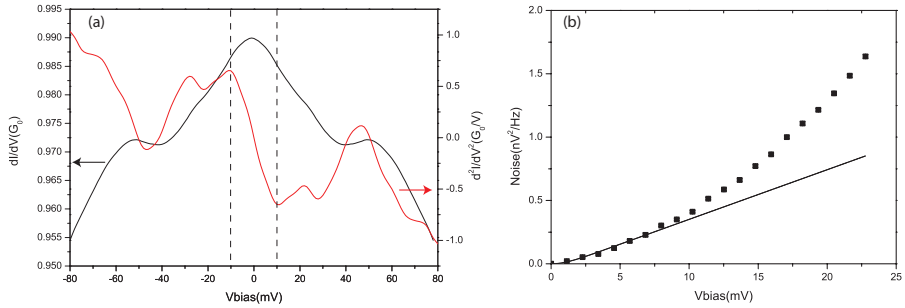

FIGURE 4.13: The non-equilibrium vibronic interaction in noise: (a) The ac conductance characterization of the atomic contact showing the differential conductance (black curve) and its derivative (red curve). The dashed line shows the position of the vibron energy *i.e.* ±10meV. (b) The inelastic shot noise spectroscopy of the Au atomic contact. The black solid line is the fit of equation(1.28). The experimental data points shows the non linear deviation above $V \geq 9.10$meV.

4

but due to the strong relaxation rate the localized vibron mode decays into bulk phonon modes before a new scattering event takes place. Hence, even at $V > \hbar\omega_0$, the local vibron mode is in equilibrium. In this case the interaction of the traversing electrons with the vibron states in equilibrium gives a correction to the noise (either positive or negative correction) that is linear in the voltage, as seen in figures (4.7 and 4.9).

Now let us consider the non-equilibrated case. When the relaxation rate of the local vibrational mode is low the electron-vibron interaction creates a non-equilibrium vibron population in the local vibrational states. Atomic chains are coupled well to the leads and hence local vibrational mode decays into bulk phonon modes. We tried to decouple an atomic chain by stretching the contact. Careful stretching of the contact either results in the pulling of a new atom into the contact or in stretching of the atomic bonds. With the MCBJ set up one can stretch the atomic contact with sub-Ångstrom precision using a piezo element. We formed a fresh atomic contact and performed high bias noise spectroscopy on the contact. Once the contact was showing a regular linear deviation in the noise above the vibron energy, the contact was stretched carefully to reduce its vibrational energy to 10meV, see figure (4.3). Once the differential conductance shows a clear vibron feature new inelastic noise spectroscopy on the contact was done. Figure (4.13) shows one example of the results. The differential conductance and its numerical derivative show a virbron energy at ±10meV for positive and negative bias. The shot noise measurement on the contact shows a non linear deviation above $V \sim 9$ meV. This observation is in contrast with the measurements shown in figure (4.7).

A non-linear deviation in the noise above the vibronic energy has been pre-

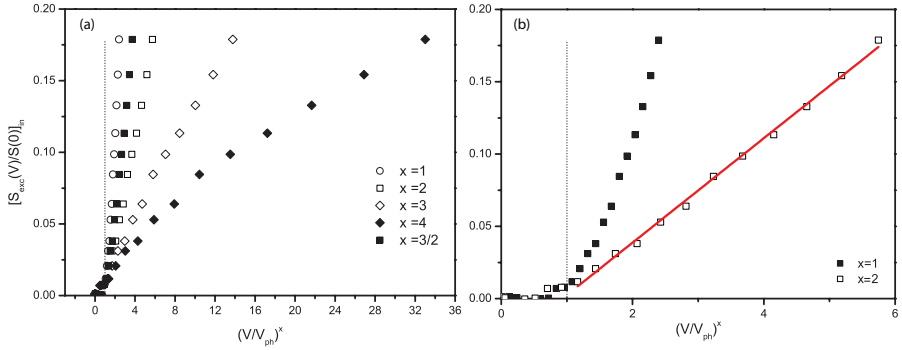

FIGURE 4.14: Evidence for non-equilibrium inelastic correction in noise: The normalized inelastic noise is plotted *w.r.t.* powers of the normalized bias voltage *i.e.* $(V/V_{ph})^x$, for $x = 1$, $x = 2$, $x = 3$, $x = 3/2$ and $x = 4$. The non-equilibrium noise shows a quadratic behavior above the vibron energy. The red line is a linear fit for the quadratic dependence.

dicted by several groups [14, 16–19]. The expected leading power varies between $V^{3/2}$[16], V^2 [14], V^3 [18], and V^4[17, 19], independent of the details of the system. We define the normalized inelastic excess noise as:

$$S_{in}(V) = (S_V(V) - S_e(V))/S(0) \tag{4.2}$$

where $S_e(V)$ is the low-bias fit to Lesovik-Levitov equation(1.28) and $S(0)$ is the thermal noise. In figure (4.14) we have plotted the inelastic noise $S_{in}(V)$ *w.r.t.* powers of normalized bias voltage *i.e.*$\left(V/V_{ph}\right)^x$ where x is the power indicated in the plot. The inelastic shot noise plot shows a good linear dependence for $x = 2$. All data sets that show non-equilibrium vibronic corrections in the noise shows powers $x = 2.0 \pm 0.1$. The experimental evidence clearly shows the feedback of the vibron fluctuations on the charge statistics of the traversing electrons. The noise increases quadratically due to this effect, which appears to agree with the predictions by Haupt and Novotny and coworkers [14]. However, the information on the actual relaxation rate of the vibron is only very indirect and it is too early to make a full comparison of the theory with the experiment.

In some of the experiments only weak non-linearities are seen above the vibron energy and sometimes slight non-linearities are seen at higher bias too. The second kink in the noise is perhaps related to the higher order of the vibron scattering process.

4.6 CONCLUSION

The inelastic interaction of the traversing electrons with the localized vibrons shows up as a jump in the differential conductance measurements. This jump in the differential conductance can be positive or negative, depending on the interplay between the opening of an inelastic channel and the availability of the final states in the lead. This gives rise the a cross over between positive and negative inelastic corrections in the conductance at $\tau = 0.5$. A related effect was predicted for noise. The noise is expected to show two cross over regimes, at $\tau_1 = 0.15$ and $\tau_2 = 0.85$, for a model system having a single conductance channel. For $0 \geq \tau \leq 0.15$ the noise should show a positive inelastic contribution, for $0.15 \geq \tau \leq 0.85$ it should show a negative inelastic contribution, and for $0.85 \geq \tau \leq 1$ again a positive inelastic contribution to the noise. Here we have investigated the cross over regime at $\tau = 0.85$. The inelastic correction to the noise is seen as a positive or a negative linear deviation from the classical Lesovik-Levitov expression, depending on the transmission probability (τ). We have proposed that the negative correction to the noise can be interpreted as a two-electron effect. The cross-over in the sign of the noise correction is seen at a slightly higher value than expected, namely at 0.95. The parameters in the model used in the theory of inelastic correction in noise are the tunneling rate Γ, the vibronic energy $\hbar\omega_0$, the electron-vibron coupling strength λ, and relaxation rate η. The cross over point does not depend on these parameters, but a shift can be found when we relax the assumption that τ is energy independent.

Due to the fast relaxation rate of vibrons in Au atomic chains the local vibron occupation is in equilibrium with the bulk phonons. This results in the linear dependence of the inelastic noise *w.r.t.* to bias voltage. In some cases where we stretched the atomic chain we have observed non-linear deviations in the noise above the vibron energy. This inelastic correction in noise shows a quadratic dependence upon normalized bias voltage (V/V_{ph}). This non-linear dependence in noise of atomic chain is quite critical to the state of stretching of chains. These effects should be more clearly pronounced in noise spectroscopy on Pt-D_2-Pt or Au-O-Au systems, where the vibrons of the molecular species are more decoupled from the bulk phonons. The non-linear dependence of the noise is due to non-equilibrium vibron fluctuations in the atomic chain. The non-equilibrium vibron produces a back action in the charge counting statistics, which could give valuable information about the phonon statistics in the molecular electronics. This can be further exploited for the determination of the lattice temperature in molecular junctions under applied bias.

REFERENCES

[1] N. Agräit, C. Untiedt, G. Rubio-Bollinger, and S. Vieira, *Onset of Energy Dissipation in Ballistic Atomic Wires*, Phys. Rev. Lett. **88**, 216803 (2002).

[2] M. J. Montgomery and T. N. Todorov, *Electron phonon interaction in atomic-scale conductors : Einstein oscillators versus full phonon modes*, Journal of Physics: Condensed Matter **15**, 8781 (2003).

[3] J. K. Viljas, J. C. Cuevas, F. Pauly, and M. Häfner, *Electron-vibration interaction in transport through atomic gold wires*, Phys. Rev. B **72**, 245415 (2005).

[4] L. de la Vega, a. Martín-Rodero, N. Agraït, and a. Yeyati, *Universal features of electron-phonon interactions in atomic wires*, Physical Review B **73**, 1 (2006).

[5] T. Frederiksen, M. Paulsson, M. Brandbyge, and A.-P. Jauho, *Inelastic transport theory from first principles: Methodology and application to nanoscale devices*, Phys. Rev. B **75**, 205413 (2007).

[6] S. Monturet and N. Lorente, *Inelastic effects in electron transport studied with wave packet propagation*, Phys. Rev. B **78**, 035445 (2008).

[7] T. Frederiksen, M. Paulsson, and M. Brandbyge, *Inelastic fingerprints of hydrogen contamination in atomic gold wire systems*, Journal of Physics: Conference Series **61**, 312 (2007).

[8] O. Tal, M. Krieger, B. Leerink, and J. M. van Ruitenbeek, *Electron-Vibration Interaction in Single-Molecule Junctions: From Contact to Tunneling Regimes*, Phys. Rev. Lett. **100**, 196804 (2008).

[9] M. Kiguchi, O. Tal, S. Wohlthat, F. Pauly, M. Krieger, D. Djukic, J. C. Cuevas, and J. M. van Ruitenbeek, *Highly Conductive Molecular Junctions Based on Direct Binding of Benzene to Platinum Electrodes*, Phys. Rev. Lett. **101**, 046801 (2008).

[10] O. Tal, M. Kiguchi, W. Thijssen, D. Djukic, C. Untiedt, R. Smit, and J. van Ruitenbeek, *Molecular signature of highly conductive metal-molecule-metal junctions*, Physical Review B **80**, 0854271 (2009).

[11] M. Taniguchi, M. Tsutsui, K. Yokota, and T. Kawai, *Inelastic electron tunneling spectroscopy of single-molecule junctions using a mechanically controllable break junction*, Nanotechnology **20**, 434008 (2009).

[12] M. Tsutsui, M. Taniguchi, and T. Kawai, *Single-molecule identification via electric current noise*, Nature communications **1**, 138 (2010).

[13] R. Avriller and A. L. Yeyati, *Electron-phonon interaction and full counting statistics in molecular junctions*, Physical Review B **80**, 0413091 (2009).

[14] F. Haupt, T. c. v. Novotný, and W. Belzig, *Phonon-Assisted Current Noise in Molecular Junctions*, Phys. Rev. Lett. **103**, 136601 (2009).

[15] T. L. Schmidt and A. Komnik, *Charge transfer statistics of a molecular quantum dot with a vibrational degree of freedom*, Physical Review B **80**, 0413071 (2009).

[16] Y. Chen, *Searching for entangled electron spin states with shot noise detection*, PhD thesis (2005).

[17] O. Jouravlev, Ph.D. thesis, Delft university of technology (2005).

[18] D. F. Urban, R. Avriller, and A. Levy Yeyati, *Nonlinear effects of phonon fluctuations on transport through nanoscale junctions*, Phys. Rev. B **82**, 121414 (2010).

[19] T. Novotný, F. Haupt, and W. Belzig, *Nonequilibrium phonon backaction on the current noise in atomic-sized junctions*, Phys. Rev. B **84**, 113107 (2011).

[20] A. I. Yanson, G. R. Bollinger, H. E. van den Brom, N. Agrait, and J. M. van Ruitenbeek, *Formation and manipulation of a metallic wire of single gold atoms*, Nature **395**, 783 (1998).

[21] C. Untiedt, a. Yanson, R. Grande, G. Rubio-Bollinger, N. Agraït, S. Vieira, and J. van Ruitenbeek, *Calibration of the length of a chain of single gold atoms*, Physical Review B **66**, 1 (2002).

[22] I. K. Yanson, *Non Linear effects in electric-conductivity of point junctions and electron-phonon interaction in normal metals*, Sov. Phys. JETP **39,**, 1974 (1974).

[23] T. Frederiksen, M. Brandbyge, N. Lorente, and A.-P. Jauho, *Inelastic Scattering and Local Heating in Atomic Gold Wires*, Phys. Rev. Lett. **93**, 256601 (2004).

[24] N. Agräit, C. Untiedt, G. Rubio-Bollinger, and S. Vieira, *Electron transport and phonons in atomic wires*, Chemical Physics **281**, 231 (2002).

[25] A. Kumar, L. Saminadayar, D. Glattli, Y. Jin, and B. Etienne, *Experimental test of the quantum shot noise reduction theory.*, Physical review letters **76**, 2778 (1996).

[26] B. Ludoph, M. H. Devoret, D. Esteve, C. Urbina, and J. M. van Ruitenbeek, *Evidence for Saturation of Channel Transmission from Conductance Fluctuations in Atomic-Size Point Contacts*, Phys. Rev. Lett. **82**, 1530 (1999).

[27] H. van den Brom and J. van Ruitenbeek, *Quantum Suppression of Shot Noise in Atom-Size Metallic Contacts*, Physical Review Letters **82**, 1526 (1999).

[28] M. Paulsson, T. Frederiksen, H. Ueba, N. Lorente, and M. Brandbyge, *Unified Description of Inelastic Propensity Rules for Electron Transport through Nanoscale Junctions*, Phys. Rev. Lett. **100**, 226604 (2008).

[29] C. Untiedt, G. Rubio Bollinger, S. Vieira, and N. Agräit, *Quantum interference in atomic-sized point contacts*, Phys. Rev. B **62**, 9962 (2000).

[30] F. D. Novaes, A. J. R. da Silva, E. Z. da Silva, and A. Fazzio, *Oxygen Clamps in Gold Nanowires*, Phys. Rev. Lett. **96**, 016104 (2006).